An approach for long-term, multi-probe Neuropixels recordings in unrestrained rats

Thomas Zhihao Luo*, Adrian G. Bondy*, Diksha Gupta, Verity A. Elliott, Charles D. Kopec, Carlos D. Brody

*These authors contributed equally.

Abstract

The use of Neuropixels probes for chronic neural recordings in freely moving animals is not yet widespread. Stable chronic recording across months has been reported from a single brain area in rats, and probe re-use has been shown for mice after an implantation period of a few weeks. These initial studies raise three questions that need to be addressed for chronic recording from freely moving animals to become cost-effective and routine. First, how does long-term yield compare across different brain regions? Second, is it possible to achieve a cost-effective strategy for freely moving animals that is i) compact enough for multiple simultaneous probes to be implanted, ii) allows probe explantation and re-use, and, importantly, iii) is robust enough for stable multi-month recordings from rats (or other animals that can generate impact forces greater than those generated by mice)? Third, how does probe performance degrade after multiple cycles of implantation? Here we address these three questions, validating an approach for chronic Neuropixels recordings over a period of months, in freely moving rats performing a cognitively-demanding task. Daily recording sessions lasted up to five hours and required no human supervision. Our approach allows for implantation of multiple probes per rat and probe recovery at the end of the experiment. We found that, on average, hundreds of units can be recorded for multiple months. However, this long-term stability strongly depended on the dorsoventral and anteroposterior position in the brain, with greater stability in more anterior and ventral regions. Finally, we quantified degradation in the performance (input-referred noise) of explanted probes after each implantation and found this degradation to be insufficient to impair future single-unit recordings. We conclude that cost-effective, multi-region, and multi-probe Neuropixels recordings can be carried out with high yields over multiple months in rats or other similarly sized animals. Our methods and observations may facilitate the standardization of chronic recording from Neuropixels probes in freely moving animals.

Introduction

Behavior depends on the concurrent spiking activity of many neurons across large distances in the brain. Therefore, tools that improve our ability to sample neuronal activity at the temporal resolution of action potentials and also with large spatial coverage will expand our ability to answer key neuroscience questions. The recent development of a silicon microelectrode array, the Neuropixels probe (Jun et al., 2017; Mora Lopez et al., 2017), is a significant step forward in that direction. Its high channel count allows sampling from hundreds of neurons per probe, on-probe amplification and digitization allows for low-noise data transmission, and a small footprint allows multiple probes to simultaneously survey regions across the brain. Given these advantages, the use of Neuropixels probes in acute experiments in head-fixed mice has become widespread and standardized (Allen et al., 2019; Steinmetz et al., 2019; The International Brain Laboratory et al., 2020).

Chronic implantations are particularly crucial for experiments that examine behaviors involving unrestrained movement, such as some perceptual decision-making (Brunton et al., 2013), exploration (Tervo et al., 2014), navigation (Ito et al., 2015), escape (Juavinett et al., 2019), foraging (Davidson and El Hady, 2019), and prey-capture (Hoy et al., 2019). However, the deployment of these probes in experiments requiring chronic implantation has remained very limited (Juavinett et al., 2019; Jun et al., 2017; Krupic et al., 2018). A previous study tracked the stability of neural signals acquired from the rat medial prefrontal cortex (Jun et al., 2017). This study found that across implants, there was no significant degradation of signals across two months. A different study reported that 20-145 single units could be isolated in the mouse visual cortex, hippocampus, and midbrain from one to two weeks after surgery (Juavinett et al., 2019). This latter study used an implantation strategy that allowed the probe to be recovered and reused, which can save laboratories substantial resources given the significant cost and limited production of the probes. Moreover, this study reported that neural signals could be observed after re-implantation of two explanted probes, but probe performance (gain and input-referred noise of electrodes) of explanted probes was not reported.

Several outstanding issues need to be addressed before the enormous potential for chronic implantation of Neuropixels probes can be fully realized. First, the long-term yield across different brain regions is unknown, because prior chronic studies recorded from a small set of brain regions using test-phase probes (Juavinett et al., 2019; Jun et al., 2017). Because the brain is not mechanically isotropic, with different viscoelastic properties and levels of respiration- and cardiac-related movement in different regions (Bayly et al., 2005; Budday et al., 2015; MacManus et al., 2018; Sloots et al., 2020), the stability of spiking signals is likely to vary across regions.

Second, the feasibility of probe reuse remains uncertain. The reusability of explanted probes was assessed previously by comparing the frequency and signal-to-noise of spiking events recorded from two re-implanted probes (Juavinett et al., 2019). However, neural signals can be highly variable, and can be different across separate implantations for reasons unrelated to the probes themselves. To assess the feasibility of probe re-use, it is necessary to also measure the performance metrics of the explanted probe, independent of neural signals. Moreover, techniques that allow probe recovery have not been validated for multi-month recordings, or validated in rats, which can be ten times larger in size than mice and can generate much larger impact forces that can damage probe signals.

To address these issues, we developed and validated an approach for recoverable chronic implants that is robust to forces generated by rats over multiple months and compact enough for multiple probes to be implanted on the same rat. We designed a compact probe holder, inspired by (Juavinett et al., 2019), that can be produced using a 3D printer and allows the probe to be easily retrieved for reuse. Using this approach, we recorded from 20 rats, each implanted with up to three probes simultaneously, while they performed a cognitively demanding task for multiple hours daily without human supervision and at a level similar to their pre-implantation baseline. Recordings were made broadly throughout the rat forebrain and midbrain. From these, we reached three conclusions: first, over a hundred well-isolated single units can be recorded per probe over multiple months. Second, the stability of long-term recording depends systematically on the dorsoventral and anteroposterior position in the brain, with greater stability for more anterior and ventral regions. This finding could guide future experiments and probe development. Finally, to test the feasibility of re-using Neuropixels probes after extended periods of implantation, we directly measured the input-referred noise of explanted probes in saline after prolonged implantation. We found only modest increases in noise across multiple (up to three) cycles of implantation and explantation, demonstrating the practicality of probe re-use. Taken together, these results further demonstrate the enormous potential of Neuropixels probes for experiments requiring unrestrained movement, and validate new methods for deploying these probes to full advantage in chronic preparations.

Results

Holder design

We developed a design for mounting and enclosing a Neuropixels 1.0 probe, with the goals to minimize the size and weight of the implant, allow the probe to be easily recovered at the end of the experiment, and be robust to impact forces that rats can generate. The design consists of an internal holder used to stereotaxically manipulate the probe and an external chassis that encases the internal holder and was cemented to the animal's head (see Methods). By unscrewing the internal holder from the external chassis, the probe can be recovered from the implant. The internal holder was attached to the probe using a dovetail joint, meaning it can be slid off, yielding a nearly bare probe after explantation. All parts were produced in-house using 3D stereolithography printers. The maximum dimensions of the assembly were 43 mm (height), 25 mm (width), and 10.5 mm (depth), with a weight of 2.6 g. The size and weight of the design provides sufficient protection to the probe from the impact force that a rat can generate while allowing for a rat to comfortably carry additional probes or hardware for neural perturbation.

Twenty rats were implanted with one or more Neuropixels probes. One rat was implanted with three probes simultaneously, and two rats with two concurrent probes (Fig. 1G,I), all enclosed in explantable probe holders. The probes targeted a large number of cortical and subcortical brain regions, including prefrontal, visual, somatosensory and retrosplenial cortex, as well as the basal ganglia, amygdala and the superior and inferior colliculi (see Methods for complete list of recording sites).

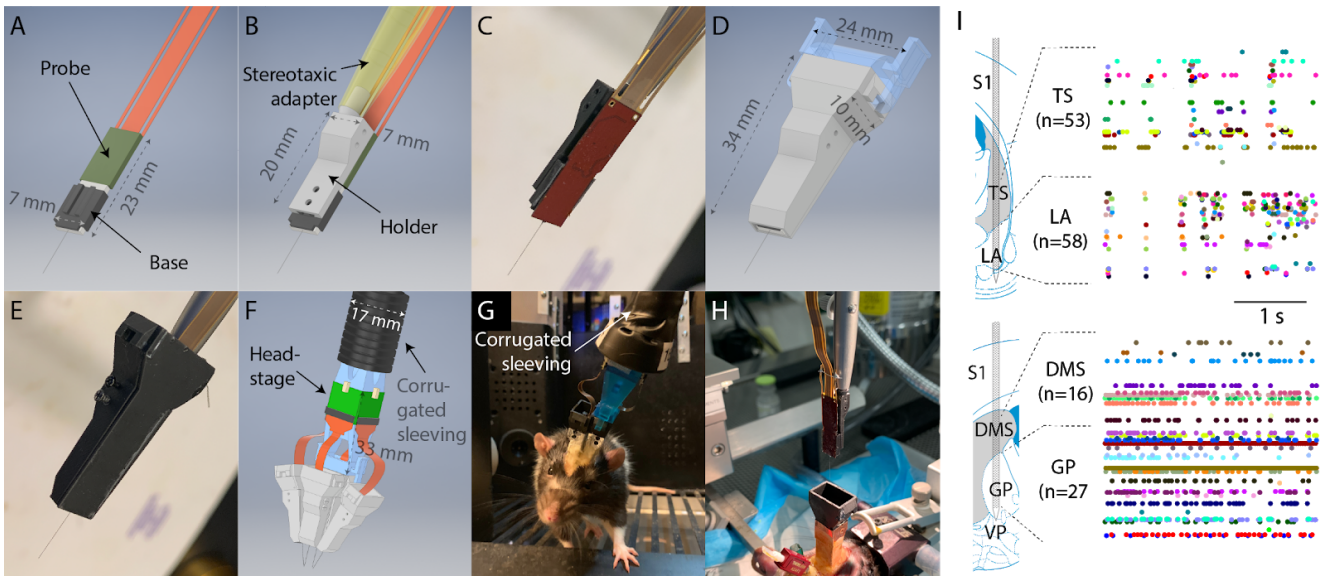

Figure 1. A compact system for chronic recording and subsequent probe recovery. To prevent bonding of the probe to the skull, the probe was fully enclosed in a chassis. During surgery, the chassis was bonded to the skull so the probe can later be detached and recovered. The assembly was sufficiently compact for multiple probes to be implanted in the same animal. A) To prepare a probe for implantation, it was first mounted to a 3D-printed base. B) Schematic of the base mating with a 3D-printed holder through a dovetail joint, and the holder was attached to a commercially available stereotaxic holder. C) A photograph of a mounted probe. D) The entire apparatus was then enclosed with a 3D-printed external chassis. During the surgery, the chassis, but not the holder, will be fixed to the skull surface using adhesive cement and acrylic, and therefore the holder can be separated from the chassis. E) A photograph of an enclosed probe, with screws securing the chassis to the internal holder visible. F) a 3D-printed headstage-mount can have up to four headstages mounted to it and mates directly with external chassis through snap-on holders. The headstage-mount was fixed to a corrugated plastic sleeving, which protects the cable from small bending radiuses. G) A rat with two probes implanted. H) A photograph of the explantation of a probe. Also visible is an interconnect for an optical fiber (red). I) Simultaneous recordings from two Neuropixels probes in a moving rat. Top: recording from tail of striatum (TS) and lateral amygdala (LA, 2.2 mm anterior to Bregma, 5.0 mm lateral). Bottom: recording from dorsomedial striatum (DMS) and globus pallidus (GP; 0.6 mm posterior to Bregma, 4.0 mm lateral). Images and schematic are adapted from (Paxinos and Watson, 2006). Colored dots indicate spike times.

Stability of spiking signals

To quantify the stability of spiking signals across days, we periodically performed short recordings of approximately ten minutes from the group of 384 electrodes either closest or second closest to the tip of the probe shank ("bank 0" and "bank 1", respectively). A total of 151 such recording sessions were performed across 20 animals and 13 unique stereotaxic coordinates. Spike sorting was performed using Kilosort2 (Pachitariu et al., 2020). To facilitate comparison across datasets and eliminate subjectivity in spike sorting (Harris et al., 2000; Wood et al., 2004), we used default parameters and no manual curation (see Methods).

We first observed that even among implants targeting the same brain area, there was substantial variability in initial and long-term signals between animals, as seen in other reports of chronic Neuropixels recording (Juavinett et al., 2019; Jun et al., 2017). For example, among three implants targeting medial frontal cortex (Figure 2A), the number of recorded single units on the day of the surgery varied by a factor of two (<200 versus >400). In two of those implants, the number of single units initially decreased and then increased, possibly due to displacement of the probe into new tissue. Variability can also be observed among implants targeting motor cortex and striatum (Figure 2B) and in implants targeting the ventral striatum (Figure 2C).

Averaged across implants, the number of isolated units (both single units and small multi-unit clusters) began at 578 ± 48 (mean ± 1 s.e.m.) on the day after implantation, decreased over the subsequent days, and stabilized after approximately one week, to approximately one half of the number of the units that can be initially recorded (8 to 120 days after implant: 292 ± 22; Figure 2D-E). After this initial loss during the first week, the number of isolated units, as well as the number of well-isolated single units, remained stable for up to four months, the longest time span for which we have sufficient data (ANOVA, single-factor (days), for only data > 7 days: tested on the number of units $p=0.738$ and on the number of single units $p=0.484$). The activity levels of the isolated units and the size of the spike waveforms also remained stable (Figure 2F-G; ANOVA, event rate: $p=0.211$; peak-to-peak amplitude: $p=0.232$). The expected yield of over 200 isolated units (100 single units) per bank per probe over the period of a week to four months after implantation indicates this approach provides sufficient signal for studying coordinated, population-level activity during behavior.

We next sought to identify the factors that influence the initial and long-term quality of spiking signals. First, we found that signal stability depends on the dorsoventral (DV) position in the brain (Figure 2H-K). The number of units recorded from the electrodes in the most superficial millimeter of brain tissue (corresponding to cortical layers I-V in all our recordings) degraded rapidly. The ratio of the average number of units >30 days after implantation to the average number of units on the first day after implantation was 0.18 (bootstrapped 95% CI = [0.08, 0.34]; same metric calculated using the number of single units: 0.13 [0.05, 0.27]). For electrodes in the second most superficial millimeter (cortical layers V-VI), the ratio was 0.23 [0.13, 0.35] (for single-units: 0.20 [0.10, 0.32]). In contrast, electrodes more than two millimeters below the brain surface, which targeted the striatum and ventral medial frontal cortex in the majority of implants, were associated with a significantly more modest level of signal degradation, with a ratio of 0.50 [0.39, 0.63] (for single units: 0.51 [0.38, 0.67]).

We sought to determine whether the dependence of signal stability on depth in the brain could be explained by the greater flexibility in the shank at distances further from the probe base. Greater flexibility was expected to result in less relative motion between the shank and the surrounding brain tissue, which is believed to be a major cause of glial scarring and signal degradation (Lecomte et al., 2018). To address this uncertainty, we leveraged the variability in the depth and angle of implantation across rats to distinguish the relative importance of position on the probe shank versus depth in the brain (dorsoventral relative to brain surface) on signal stability. To do this, units from each session were grouped by whether they were recorded from an electrode in bank 0 or bank 1, although conclusions were similar if shank positions were binned into

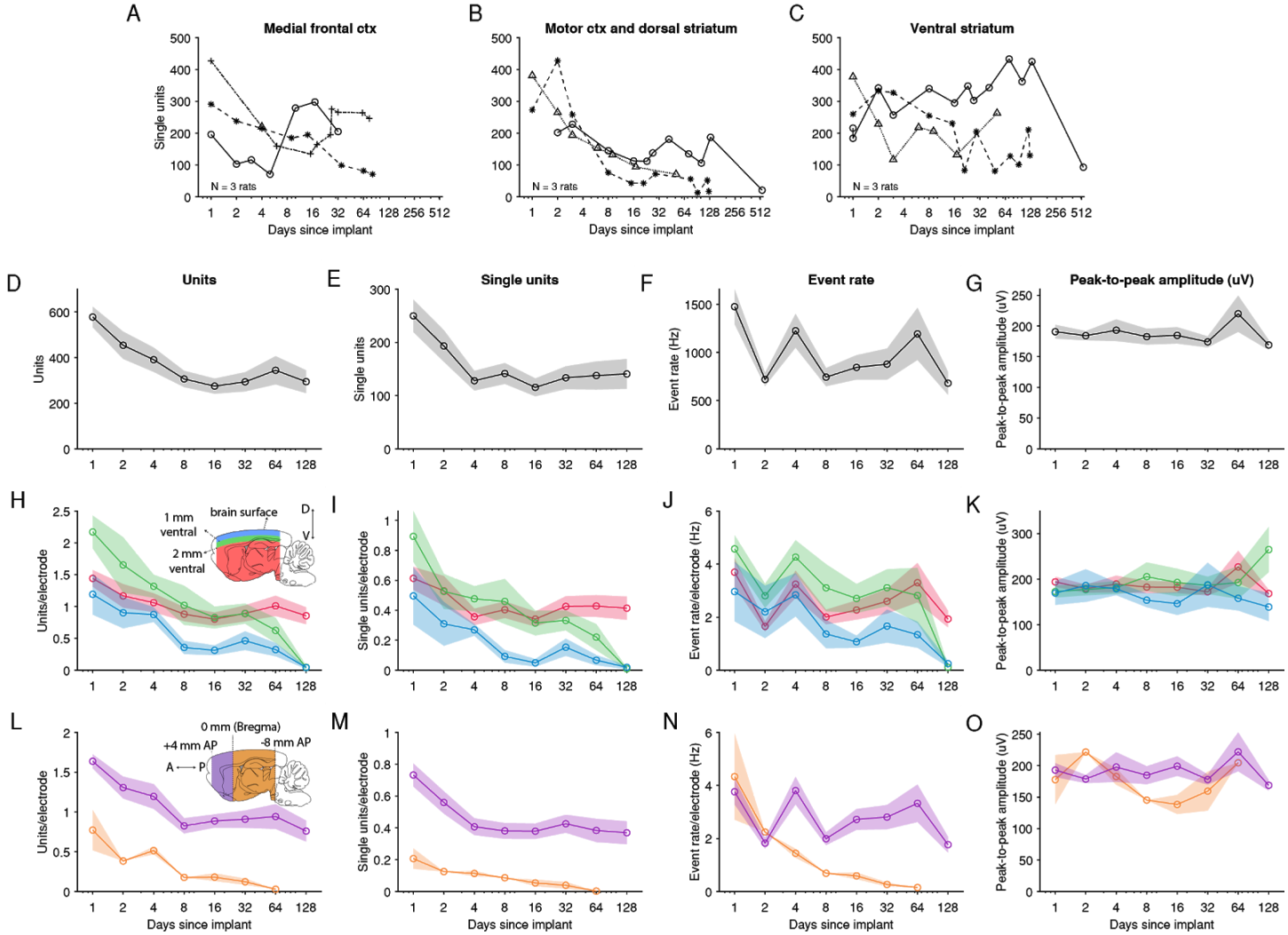

Figure 2. After an initial loss of units, spiking signals can be maintained >60 days in anterior, deeper brain regions. A) Recordings from the medial frontal cortex (including secondary motor, cingulate, prelimbic, and medial orbital cortices) across three animals. Each combination of marker and line types indicates one animal. B) Recordings from secondary motor cortex and anterior dorsal striatum C) Recordings from anterior ventral striatum. D) The number of isolated units recorded. Shading represents mean +/- 1 s.e.m. across recording sessions. E) The number of single units. F) The total number of spikes detected across all units. G) The average peak-to-peak amplitude of waveforms. (D-G) N = (12, 8, 20, 19, 33, 20, 17, 16) recording sessions for each bin. H) The number of units recorded at different positions along the dorsal-ventral (DV) axis of the brain for each recording session, normalized by the number of recording electrodes at those positions. I-K) same as E-G, but grouped based on unit positions. (H-K) DV [-1, 0] mm: N = (7, 4, 9, 8, 13, 10, 9, 5). DV [-2 -1] mm: N = (7, 4, 11, 8, 15, 10, 10, 5). DV [-10, -2] mm: N = (12, 8, 20, 19, 33, 20, 17, 16). L-O) Units are grouped according to their position along the anterior-posterior axis of the brain. AP [0, 4] mm: N = (11, 7, 16, 18, 25, 16, 16, 16). AP [-8, 0] mm: N = (2, 1, 5, 1, 8, 4, 1).

more groups. Units were also sorted by their depth below the brain surface in the same bins shown in Figure 2H. The neuronal yield was computed for each pair of conditions (shank position and brain depth) and then normalized by the number of electrodes in the same group. To index signal loss, we calculated the change from the initial recordings (maximum number of units during the first five days of recording) and late recordings (average of recordings four to twenty weeks after implantation). An ANOVA was performed on this change in unit count, using as main factors shank position (bank 0 or bank 1) and brain depth. We found a significant effect of brain depth ($p=0.009$) but not shank position ($p=0.667$). Similar results were found for the metric of number of single units (brain depth: $p=0.017$; shank position: $p=0.967$) and event rate (brain depth: $p=0.017$; shank position: $p=0.839$). This additional analysis indicates that the observed relationship between yield stability and depth must depend on factors other than the gradient in flexibility along the shank (see Discussion).

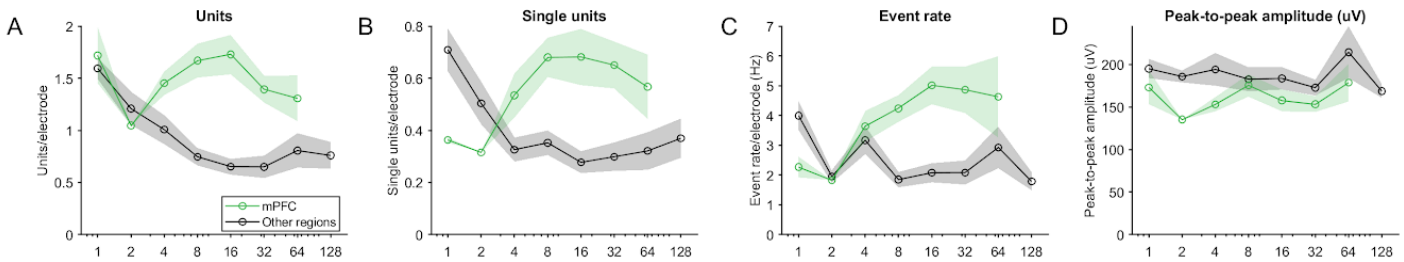

Figure 2--figure supplement 1. **No degradation of spiking signals was detected over two months in rat medial prefrontal cortex (mPFC), the brain region in which the stability of spiking signals was examined in (Jun et al., 2017)**. mPFC was recorded from four probes (one probe/animal, N = 2, 1, 6, 3, 4, 6, 4 sessions, implanted 4.0 mm anterior to Bregma, 1.0 mm lateral, 10° in the coronal plane at the probe tip relative to DV axis) and from the electrodes of those probes located in prelimbic cortex or medial orbital cortex, as according to probe tracks in histological slices and referenced to (Paxinos and Watson, 2006). This finding contrasts with the clear signal degradation at all other recording sites. (A) The number of single units normalized by the number of electrodes in that brain region. (B) The number of single units. (C) The event rate. (D) The average peak-to-peak amplitude of waveforms.

We also found that the quality and stability of neural signals depended greatly on the probe's position along the animal's anteroposterior (AP) axis (Figure 2L-O). We observed a pronounced difference between our recordings anterior and posterior to Bregma. Recordings from more posterior sites were associated with fewer initial clusters (*p=0.010*, rank-sum test), which could be in part due to a lower neuron density in the posterior structures compared to the anterior structures that we recorded from (Erö et al., 2018). There was also a more severe degradation in yield in the posterior areas, with a virtually complete loss of units after one month. The ratio of the number of units >30 days after implantation to the unit count 1 day after implantation was 0.09 (95% CI = [0.04, 0.22]) for posterior recordings and 0.45 [0.36, 0.57] for the anterior recordings. The same ratio for the number of single units was 0.06 [0.00, 0.21] for posterior recordings and 0.45 [0.34, 0.59] for anterior recordings. There is likely more granularity for the measurements posterior to Bregma, but our data are not sufficiently powered to characterize it. For the larger set of recordings anterior to Bregma, we did not observe a significant dependence of signal stability on AP position (data not shown). Lastly, our recordings were not sufficient to address whether there was a dependence of signal stability of ML position.

The loss of spiking signals that we observe at first appears to contrast with a previous study reporting chronic recording in rat medial prefrontal cortex (mPFC) (Jun et al., 2017), where no such loss was found. However, when we examine just the mPFC recordings in our dataset (prelimbic cortex and medial orbital cortex, n=5 rats), no degradation in the number of units was apparent over a two month span, and the number of single units and event rate actually increased (Figure 2--supplement 1). This finding further demonstrates the dependence of signal stability on anatomical AP and DV positions, because our recordings from mPFC were the most anterior (AP = 4.0 mm from Bregma) and were taken 1.8 mm or more below the brain surface.

Behavioral performance while tethered for recording

Our motivation to chronically implant Neuropixels probes was to study coordinated neural activity during perceptual decision-making, and therefore, we sought to determine in what ways the recording procedure might change the animals' behavioral performance. In our approach, the cable connecting the headstage and the IMEC base station was encased in a split corrugated sleeving to limit the number of turns an animal can make in a single direction to three to five and thereby avoid small bending radiuses in the cable during hours of unsupervised recording (Figure 1F-G). We sought to quantify the effects of the tether's movement restriction on performance.

During the perceptual decision-making task, rats maintained their nose in a center port while two streams of auditory clicks played from loudspeakers on their left and right (Brunton et al., 2013). When the auditory stimulus ended, rats were rewarded for reporting which stream had played the greater number of

clicks by placing their nose in a left or right port (Figure 3A). We found little or no significant degradation in a number of critical metrics of behavioral performance between when the rats were untethered and when they were tethered for recording. The median number of trials for which the rat was able to successfully maintain fixation in a given session remained similar (Figure 3B), indicating that the additional weight and constraint of the implant and tether did not affect the number of completed trials. The average percent correct was actually slightly higher during tethered performance, although not significantly so (Figure 3C). The performance of individual rats was further quantified using a logistic function fit to their choice and the sensory evidence in each trial (Figure 3D; Methods). The slope of the logistic function (at the midpoint), which quantifies sensitivity to the sensory evidence, and the bias parameter were not significantly different (Figure 3E-F). Interestingly, tethered performance was associated with a lower lapse rate (Figure 3G). The lower median lapse rate could potentially be because after the surgery, the rats performed the task more frequently while tethered than untethered and therefore are more engaged while tethered and showed higher performance. These results indicate that the tethering process did not substantially impair the rats' motivation or their ability to successfully complete a cognitively demanding task.

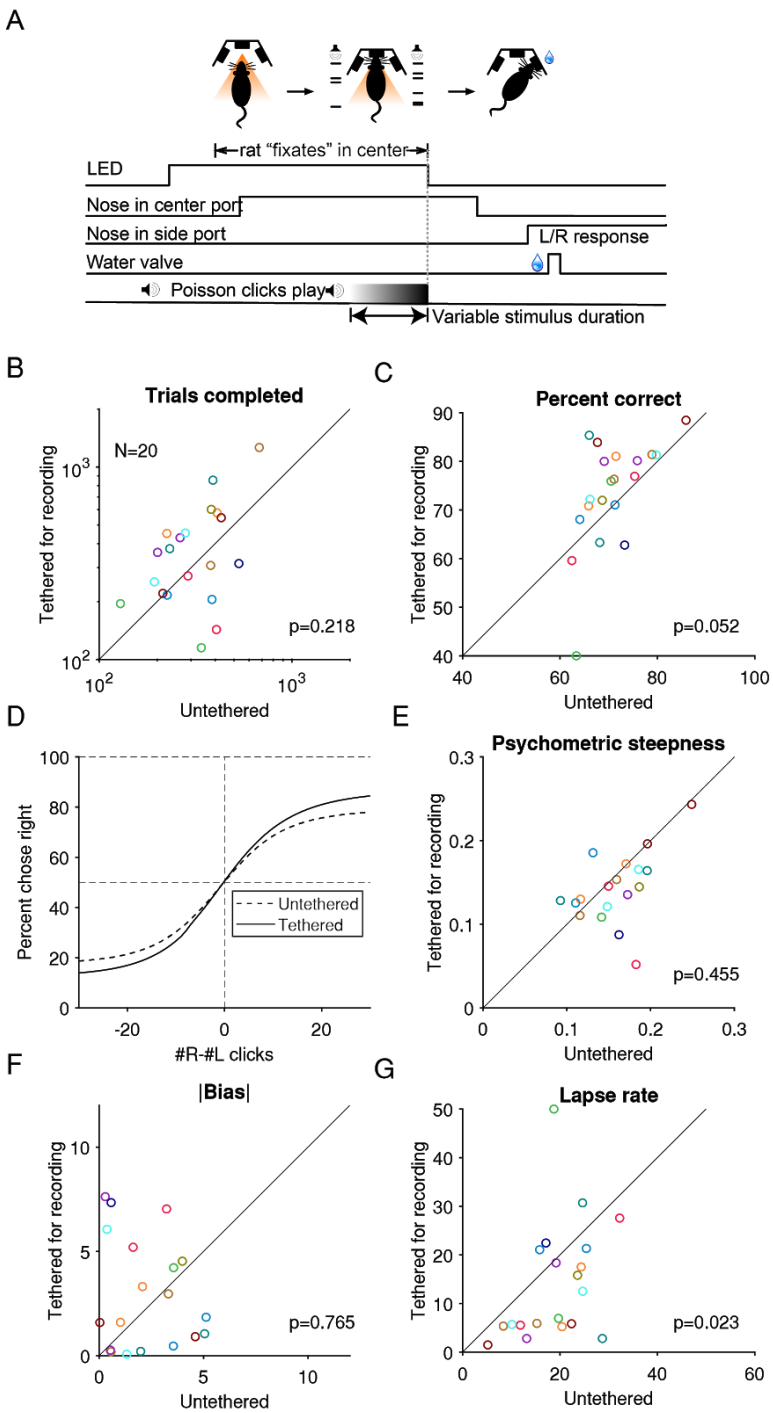

Figure 3. While tethered for Neuropixel recording without a cable commutator, rats perform a cognitively demanding task at a level similar to when they are untethered. A) Task schematic: rats hold their nose in the center port while listening to two concurrent streams of auditory clicks, one from a loudspeaker to its left and the other to its right. At the end of the stimulus, the rat receives a reward if it oriented toward the port on the side where more clicks were played. Adapted from (Brunton et al., 2013). B) The median number of trials completed by an animal in each training or recording session, compared between tethered and untethered. Each marker indicates an animal. P-values are based on the null hypothesis that the median difference between paired observations is zero and calculated using the Wilcoxon signed-rank test. C) The percentage of trials when an animal responded correctly. D) Logistic curves fitted to data pooled across from all animals. E) Comparison of the behavioral psychometric curves' steepness parameter (slope of the sigmoid at the inflection point). G) Absolute value of the bias parameter. F) The average of the lapse rate. A larger lapse indicates a larger fraction of trials when the animal was not guided by the stimulus or a decreased ability to take advantage of large click differences.

Probe reuse

Previous work reported that reimplantation of two test-phase Neuropixels probes resulted in a lower event rate and signal-to-noise of detected spikes (Juavinett et al., 2019). However, event rate and signal-to-noise in the brain depend not only on probe performance but also on variability in the recording site itself. Therefore, it remains unclear to what extent probe performance degrades after prolonged implantation and explantation. Addressing this uncertainty is necessary for determining whether probe reusability is feasible.

We measured the change in the input-referred noise (i.e., noise divided by gain) in saline and compared these measurements between explanted probes and probes that have never been implanted (Methods). Only the electrodes on the segment of the probe shank that was implanted in the brain were analyzed because overlying electrodes were covered with silicone elastomer or petroleum jelly during the surgery, which could not be fully removed. In a probe that was explanted after 123 days, we found that the noise was typically less than 10 uV (median across electrodes = 9.3 μV and 2.5 and 97.5 percentiles = [7.3, 14.9] μV; Figure 4A). These values are similar to those of an example new probe (8.6 μV and [6.9, 14.2] μV; Figure 4B).

Comparing between the measurements from three probes that have never been implanted and from five probes after their most recent explantation, we detected slightly larger noise values in explanted probes (median = 8.30 μV; n = 3664 electrodes) compared to new probes (median = 8.10 μV; n = 2880 electrodes; p=0.043 Wilcoxon rank-sum test; Figure 4C). Importantly, this increase is two orders of magnitude less than the median peak-to-peak amplitude of the spikes that were detected (188 μV; 2.5 and 97.5 percentiles = [38, 624] μV across units; Figure 2G). We further examined the fraction of “noisy” electrodes (which we arbitrarily classify as noise > 20 uV (Figure 4D) and found a detectable but minor increase in the explanted probes (mean and 95% CI: 0.40% and [0.22%, 0.73%] across all new probes tested compared to 1.35% and [1.03%, 1.74%] across explanted probes).

Because of the minor degradation between new and explanted probes, reimplantation is expected to have at most a minor impact on the quality of the neural signals. Consistent with this expectation, one probe was implanted in the medial frontal cortex of thee animals, and the neural quality metrics of the initial, second, and third implantations did not show a trend of increasing degradation (Figure 4E-H; ANOVA, one-way (the number of previous implants), tested on the number of units (*p=0.348*), the number of single units (*p=0.362*), the event rate (*p=0.433*), and the peak-to-peak amplitude (*p=0.767*)). Analysis of neural responses during the decision-making task (Figure 3A) indicates that similar signals can be observed across implantations. Neurons in dorsal medial frontal cortex show task-related selectivity for the animal’s choice, more strongly than in ventral medial frontal cortex (Luo et al., 2020). This pattern of selectivity can be observed across the recordings from the same probe implanted in different animals (Figure 4I-K), and the choice selectivity averaged across units was similar between the first and third implant (Figure 4L; ANOVA, one-way (the number of previous implants), tested on the the peak choice selectivity across neurons, *p=0.382*). These results indicate the minor increases in noise level across repeated cycles of implantation and explantation of the same probe did not prevent acquisition of high-quality spiking signals.

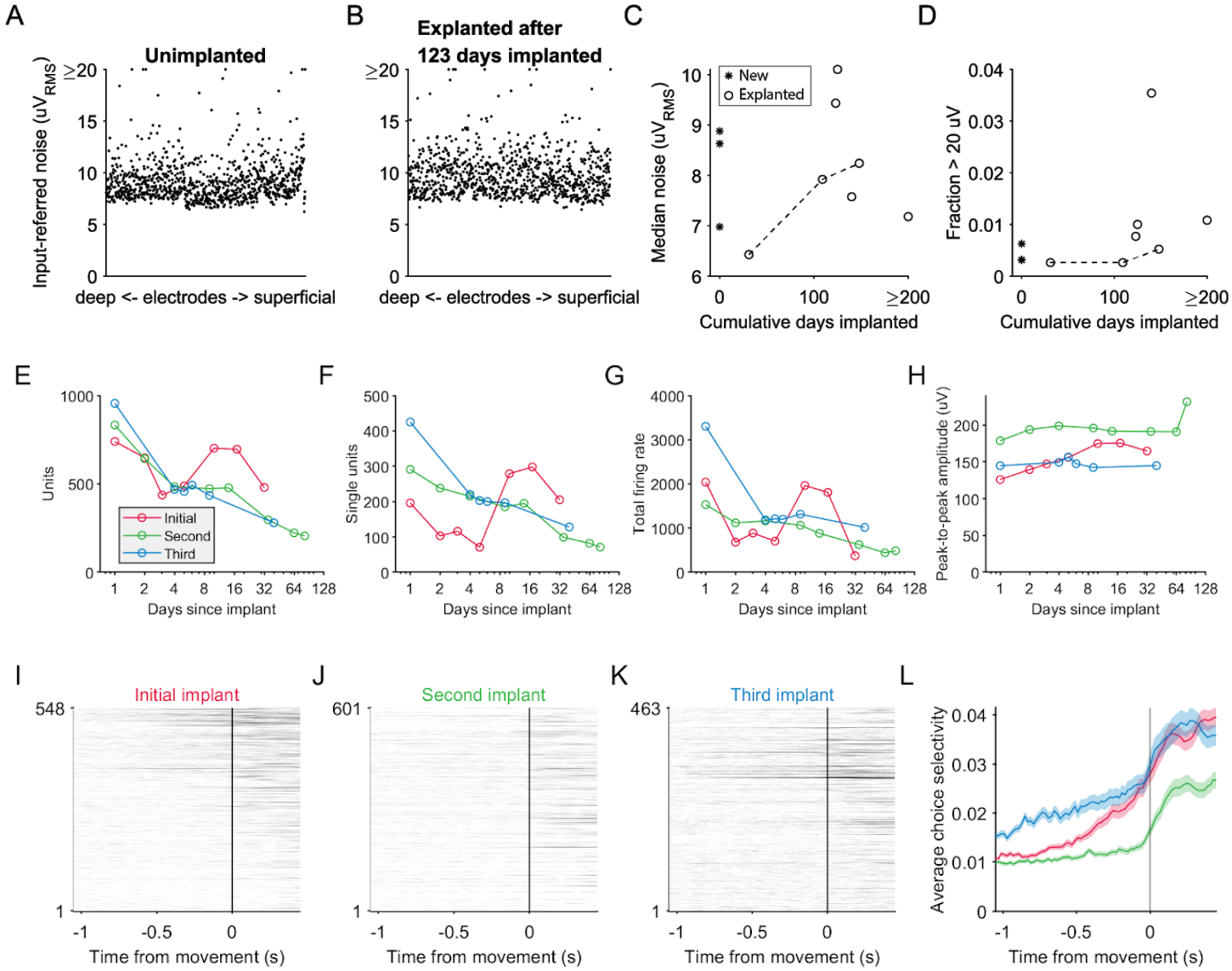

Figure 4. Explanted probes and unimplanted probes have similar input-referred noise and can acquire neural signals of similar quality. A) The input-referred noise (i.e. noise divided by gain) of each of 960 electrodes of an unimplanted probe measured in saline. B) The noise of a probe explanted after 123 days. C) The median noise across electrodes on the portion of the probe shank that were implanted in the brain. Data from one probe that was implanted in three different animals is connected by a dashed line. D) The fraction of channels with a noise value greater than 20μV_{RMS}. E-H) Signal quality of the same probe implanted in the medial frontal cortex of three separate animals. (I-K) Choice selectivity of spike counts of isolated units from three recording sessions from the same probe, each in a separate animal. Units are ordered from its relative anatomical position along the dorsal-ventral axis (superficial: top) L) Choice selectivity averaged across units did not diminish across successive implants. Shading indicates mean +/- 1 s.e.m.

Discussion

We sought to address three issues that have slowed widespread use of Neuropixels probes for chronic implantation in freely moving animals. First, the expected yield over multiple months is known for only a single brain area. Second, methods currently do not exist for implanting Neuropixels probes in a highly compact form factor, compatible with probe explantation, and robust enough to ensure high yields after months on a rat or other similarly sized animal. And third, the performance of explanted probes compared to unimplanted probes remains unclear. Here, inspired by previous approaches for chronic Neuropixels implants (Juavinett et al., 2019; Jun et al., 2017) , we report a system for chronic implantation of Neuropixels probes in rats that is sufficiently compact for multiple probes to be simultaneously implanted, robust enough to withstand months of implantation and hours of unmonitored recording per day, and compatible with probe recovery and reuse. We validated the system in 20 rats and documented the performance of the chronic implants over many months. Encouragingly, we found that on average, the degradation of spiking signals occurred during the first week of recording and then remained stable for up to four months. However, stability varied systematically according to brain region, with greatest stability in anterior and ventral brain regions. During recording, even with a restriction on movement imposed by a non-commutated tether, rats performed a cognitively demanding task at a level similar to their untethered performance before implantation. Lastly, we demonstrate that after multiple months of implantation, explanted probes show a decrease in performance, but of a magnitude unlikely to have detectable consequence on acquisition of spiking signals. These results provide practical considerations that can facilitate further adoption, standardization, and development of Neuropixels probes for chronic recording in unrestrained animals.

Long-term stability of neural signals

We found a gradual degradation of spiking signals, with slower degradation in more anterior and more ventral regions (Figure 2). The degradation is likely in part due to an inflammatory response of the tissue adjacent to the implant, consisting of activation of glia and resulting in the encapsulation of the microelectrode (Lecomte et al., 2018). It is thought that activated glia, whose markers can be elevated up to 0.5 mm from the implant interface (Kim et al., 2004), insulates the neurons from the microelectrode surface and thereby reduces the recorded voltages. Causes for the glial activation include micromotions of the brain tissue adjacent to the implant caused by respiration and cardiac pulsatility (Muthuswamy et al., 2005) and also inertial forces caused by head acceleration, resulting from the density difference between the implant and the tissue (Lind et al., 2013). The micromotions arise in part due to the more than three orders of magnitude difference in elasticity modulus between silicon microelectrode probes and that of nervous tissue (Lecomte et al., 2018). Future probe designs that allow for a greater mechanical flexibility could substantially improve the longevity of the signals (Chung et al., 2019; Jeong et al., 2015; Kim et al., 2004; Luan et al., 2017; Polikov et al., 2005).

The dependence of signal stability on anatomical position may be related to inter-regional differences in the viscoelastic properties of nervous tissues and amount of tissue micromotion. Differences in tissue elasticity have been observed across different structures in the brain (MacManus et al., 2018) and between white and gray matter (Budday et al., 2015), but a comparison between anterior and posterior cortex of the pig brain did not show a difference in elastic modulus (Gefen and Margulies, 2004). It is therefore uncertain to what extent differences in elastic moduli of brain tissue could explain the dependence of the stability of spiking signals on the anatomical position. The micromotion in the tissues adjacent to a silicon probe is on the order of tens of microns even during rest, due to pressure changes during respiration (Gilletti and Muthuswamy, 2006), and is likely larger during head acceleration (Zhou et al., 2020). Because regional differences in tissue micromotion can be observed in the human brain related to respiratory and cardiac pulsatility (Sloots et al., 2020) or related to head acceleration (Bayly et al., 2005). It is therefore possible that inter-regional differences in the amount of

tissue micromotion during breathing and head acceleration contribute to the differences in the stability of spiking signals.

Damage caused by the durotomy and the probe insertion may contribute to the loss of spiking signals in superficial brain regions, as well as the significant variability across implantations in signal quality. The amount of brain micromotion around an implant increases when the dura is removed (Muthuswamy et al., 2005), and superficial brain tissue is closer to the dural opening may experience greater micromotion and therefore greater glial activation. In addition, the implantation procedure necessarily constitutes an acute injury to the skull and meninges proximal to superficial cortex, and the insertion of even a sharp silicon probe into brain tissue can rupture, sever, and drag blood vessels and deform the tissue (Bjornsson et al., 2006). The nature and extent of these injuries were likely variable across implantations, in ways we did not attempt to carefully characterize. This trauma, and the related tissue response, may have contributed to the decreased stability specific to superficial cortex, as well as the variability in signal quality across implantations.

Holder design

Compared to a previous design for recoverable, chronic implantation of Neuropixels probes (Juavinett et al., 2019), we aimed for different experimental goals and therefore made different design choices. A primary goal was to ensure the probe was protected from the mechanical stresses in a multi-month implant on a large rodent. For this reason, the probe was fully enclosed with a 3D printed chassis which could be strongly cemented to the skull and dampen impacts. To maximize the number of probes that can fit on a single animal, a mount for the headstage was placed on top of the probe rather than to its side. Additionally, the cross-section of the external chassis close to its ventral face was minimized to allow probes to be inserted at a large range of angles. This change greatly facilitates multi-probe implantations. Lastly, the chassis and the holder were held together using screws rather than acrylic. One possibility this allows is to move the probe relative to the chassis to try to dissociate the probe from glial scar, and in a few probes for which this was attempted, an increase in signal could be observed.

Many designs of chronic implant of silicon probes or tetrodes involve a drive to move the sensor into new tissue to obtain new signals after scar tissue has accumulated (Bragin et al., 2000; Chung et al., 2017). We opted to not use a drivable design because we found that the electrodes above the brain often show a degradation in performance (i.e. higher input-referred noise) due to coverage by the possible combination of silicone elastomer, petroleum jelly, or dried blood or cerebrospinal fluid. Unlike tetrodes or other silicon probes, which have their electrode sites at the bottom of the probe, the electrodes on the Neuropixels are along the shank. Therefore, a driveable mechanism would primarily improve signals in ventral brain areas, at the expense of signals in the dorsal areas, by driving electrodes immersed in dorsal brain regions into ventral brain areas and driving electrodes above the brain, which we observed to show signal degradation, into the dorsal areas. Because our experimental goals involve simultaneous monitoring of both ventral and dorsal brain areas, we did not choose to use a driveable design. But other experiments might benefit from a driveable design.

Conclusion

Chronic implantation of microelectrodes has been and will likely continue to be an essential technique in neuroscience. However, the Neuropixels probe--a major advance in the electrophysiological toolkit--has not yet reached its full potential due to technical obstacles associated with long-term chronic implantation. The system described here represents a significant step forward in overcoming these obstacles and achieving highly stable, cost-effective, and parallel recordings from chronically implanted Neuropixels probes in freely moving animals. Our characterization of this system may also serve to inform future development of new electrophysiological probes for chronic use as well as improve implantation methods for species and experimental needs not considered here.

Methods

Subjects

A total of 20 male Long-Evans rats (*Rattus norvegicus*) were used in this study. Four of them were BAC transgenic rats expressing Cre recombinase. These rats were used for the purpose of targeting optogenetic constructs to cell types of interest for experiments not described in the present report. These rats came from the following three lines: LE-Tg(Pvalb-iCre)2Ottc (n=1), LE-Tg(Gad1-iCre)3Ottc (n=2), LE-Tg(Drd2-iCre)1Ottc (n=1). These lines were made by the Transgenic Rat Project at the National Institute of Drug Abuse (NIDA) and were obtained from the Rat Resource and Research Center (RRRC) at the University of Missouri.

All rats were water restricted to motivate them to work for water as reward, and obtained a minimum volume of water per day equal to 3% of their body mass. If rats consumed less than this minimum during performance of the task, additional water was offered after training. Rats were kept on a reversed 12-hr light-dark cycle and were trained in their dark cycle. Rats were pair housed whenever possible during early training, but were always single housed after implantation to prevent damage to the implant. Starting from the day before each surgery to at least three days after the surgery, rats were given ab lib access to water. Animal use procedures were approved by the Princeton University Institutional Animal Care and Use Committee and carried out in accordance with National Institute of Health standards.

Holder design

All probes used were commercially available Neuropixels 1.0 probes (IMEC), with the option of a flat silicon spacer attached parallel to the plane of the probe. To prepare a probe for implantation, the silicon spacer was first glued to a 3D-printed plastic base with dovetail rails, inspired by the stainless steel dovetail rails now optionally shipped on the probes. This dovetail connection mated with matching dovetail rails on an internal holder that could be manipulated using a stereotaxic holder (Kopf, Model 1766-AP Cannula Holder). The gold pads on the probe flex cable corresponding to ground and external reference were shorted by soldering a 0.01” silver wire to them. The entire apparatus was then enclosed with a 3D-printed external chassis and the holder and the chassis were connected using screws. The chassis was then wrapped in conductive tape to provide electromagnetic shielding and coated in a thin layer of C&B Metabond (Parkell, Inc) for better adherence to the dental acrylic during implantation. The bottom surface of the chassis was sealed with petroleum jelly, dispensed in liquid droplets from a low-temperature cautery (Bovie), to prevent blood from entering the chassis after implantation. During the surgery, after the probe was inserted into the brain, the chassis, but not the holder, was fixed to the skull surface using adhesive cement and acrylic. The internal holder did not come into contact with the adhesives and therefore can be detached from the chassis by removal of the screws.

During recording, a 3D-printed “headstage-mount” mated directly with the chassis through a latching mechanism, and mounted headstages were connected to the flex cable of a probe. Up to four headstages can be mounted so that up to four probes can be simultaneously implanted and recorded using this system. (Although, note that the size and geometry of the implant places constraints on the set of coordinates that can be simultaneously targeted, constraints that become more significant when more probes are implanted at once). The recording cables were placed inside a corrugated plastic sleeving to avoid small bending radiuses (1/2” internal diameter, McMaster 7840K73). This sleeving was permanently attached to the recording cap using electrical tape.

All parts except the probe itself and the screws were 3D printed in-house using Formlabs SLA printers (Form 2 and Form 3). Prints used standard black Formlabs resin, except for the recording cap which was printed in “Tough” Formlabs resin, required for the flexible latching mechanism.

A subset of implants (n=6) were made using an earlier version of the 3D design that embodied a similar design principle but were slightly larger in size. Results were similar between the two versions of the design and were therefore combined.

CAD files, detailed protocols for implant assembly and surgeries, code, and data are provided at https://github.com/Brody-Lab/chronic_neuropixels.

Implantation

Surgeries were performed using techniques that were similar to those reported previously (Erlich et al., 2011). Rats were placed in an induction chamber under 4% isoflurane for several minutes to induce anesthesia and then injected with 10 mg ketamine and 6μg buprenorphine intraperitoneally to further assist induction and provide analgesia. Rats were then placed on a stereotaxic frame (Kopf Instruments) and anesthesia was maintained with 1-2% isoflurane flowing continuously through a nose cone. After verifying surgical levels of anesthesia, rats were secured in ear bars, shaved and cleaned with ethanol and betadine. A midline incision was then made with a scalpel and a spatula was used to clean the skull of all overlying tissue.

A small, crater-like craniotomy roughly 1mm in diameter was made at the site of probe implantation. A needle was used to cut an approximately 0.5 mm slit in the dura into which the probe was later lowered. This procedure was repeated at the site of each probe to be implanted. Next, a craniotomy and durotomy were performed at a site distal to the brain region(s) to be recorded, typically in the olfactory bulb or cerebellum, into which a ground (wire, pin, or cannula) would later be inserted. Saline soaked Gelfoam (Pfizer Injectables) was placed in the craniotomies to protect the brain while a thin coat of C&B Metabond (Parkell, Inc) was applied to the skull surface. Then, the Gelfoam was removed from the ground craniotomy and the ground was lowered into the brain. This craniotomy was then sealed with Kwik-Sil (WPI) and the ground was fixed in place using a small amount of dental composite (Absolute Dentin, Parkell, Inc.).

Gelfoam was removed one by one from the remaining craniotomies and the probes inserted. Probes were manually lowered at a rate of 0.1 mm every 10-30 s. After a probe was fully inserted, a small quantity (<5uL) of soft silicone gel (DOWSIL 3-4680, Dow Chemical) was injected to seal the craniotomy. We found that harder silicones, such as Kwik-Sil (WPI), could damage the probe shank upon application. Dental composite (Absolute Dentin, Parkell) was then used to create a wall-like barrier covering the gaps below the four ventral edges of the external chassis and the skull, creating a seal around the probe shank. After these steps were completed for each probe, the silver wires soldered to the ground and external reference pads on each probe flex cable were then soldered to the common animal ground. Acrylic resin (DuraLay, Reliance Dental) was applied to secure the entire implant assembly to the Metabond-coated skull. Rats were given ketoprofen after the surgery and again 24 and 48 hours post-operative and recovered with ad lib access to water for 5 days before returning to water restriction.

List of Implantation Sites

The table below details the coordinates of each probe insertion site, relative to Bregma. A positive angle in the coronal plane indicates that the probe tip was more lateral than the insertion site at the brain surface, and a positive angle in the sagittal plane indicates that the probe tip was more anterior than the insertion site.

AP (mm)	ML (mm)	Depth (mm)	Angle in the coronal plane (°)	Angle in the sagittal plane (°)	Brain regions	Number of implanted probes
4.0	1.0	4.2	-10	0	Medial frontal cortex (secondary motor cortex, cingulate cortex, medial prefrontal cortex (prelimbic and medial orbital cortices))	5
2.2	2.1	6.8	-5	0	Secondary motor cortex, anterior dorsal striatum, anterior ventral striatum	1
1.9	1.3	8.2	15	0		3
1.9	0.8	7.0	20	0		1
1.0	2.4	7.9	0	15		4
0.8	4.0	6.6	-2	0	Somatosensory cortex, dorsomedial striatum	1
0.7	2.45	9	0	0	Preoptic area, amygdala, ventral pallidum, globus pallidus, dorsomedial striatum, motor cortex	1
0.7	2.15	10	2	0	Preoptic area, bed nucleus of the stria terminalis, dorsomedial striatum, motor cortex	1
-0.6	4.0	10	-2	0	Somatosensory cortex, posterior dorsomedial striatum, amygdala	1
-2.35	4.95	7.6	5	0	Somatosensory cortex, striatum tail, amygdala	1
-6.6	1.6	7.8	-40	0	Primary visual cortex, retrosplenial cortex, superior colliculus, and inferior colliculus	1
-6.8	1.7	8	-40	0		1
-7.0	3.0	5.8	0	0	Primary visual cortex, postrhinal cortex, and inferior colliculus	1

Explantation

To explant a probe, the animal was first anesthetized and placed in the stereotaxic frame. Then, a stereotaxic arm was attached to the probe's internal holder and the screws fixing the internal holder and external chassis were removed. The stereotaxic arm was raised until the internal holder, carrying the probe, was fully removed. The internal holder sometimes adhered to the external chassis after screw removal. In these cases, the external chassis was carefully drilled away with a dental drill until the internal holder could be

easily removed. After explantation, the probe shank was fully immersed in 1% tergazyme (Alconox) for 24-48h, followed by a brief rinse in distilled water and isopropyl alcohol, in that order.

Due to skull degradation, especially on animals with multiple survival surgeries, a subset of implants detached before the end of the experiment. Similar skull degradation could be observed for animals with other implants, such as tetrode drives. In addition, we have observed both unimplanted and implanted probes to fail due to unidentified electronic issues. All other probes could be explanted.

Electrophysiological recordings

Electrophysiological recordings were performed using either commercially available Neuropixels 1.0 acquisition hardware (Putzeys et al., 2019) or earlier test-phase IMEC acquisition hardware. The former was used in conjunction with PCI eXtensions for Instrumentation (PXI) hardware from National Instruments (including a PXIe-1071 chassis and PXI-6133 I/O module for recording analog and digital inputs.) For measurement of signal stability over time, the selected reference was a silver wire shorted to the ground wire and penetrating the brain at a different location from the probe insertion site. The amplifier gain used during recording was 500. The recording channels addressed either the deepest 384 electrodes ("bank 0") or the second deepest 384 electrodes ("bank 1"), and recordings lasted approximately ten minutes. Recordings were made on days with logarithmically-spaced intervals.

Spikes were sorted offline using Kilosort2 (Pachitariu et al., 2020), using default parameters and without manual curation. A unit was considered a single-unit if Kilosort2 categorized that unit as "good." A putative single unit meets both of the following conditions: 1) the proportion of refractory violations was less than 0.05. This proportion was computed by calculating a unit's autocorrelogram in one millisecond bins, summing the values in the central bins, and normalizing the sum by the expected sum from the mean firing rates. This normalized value was compared to a normalized sum similarly calculated from the shoulder of the autocorrelogram. The span of the central bins range varied from +/-1.5 ms to +/-10.5 ms, and a separate ratio was computed for each span. The span of the shoulder bins were either +/-10.5 ms to +/-50 ms or +/-25.5 ms to +/-499.5 ms. A separate ratio was calculated for each combination central bin span and shoulder bin span. The minimum ratio across combinations was the proportion of refractory violations. 2) For each span of central bins, a probability was calculated for the number observed coincidences in the central bins of the autocorrelogram, or fewer, being produced by a Poisson distribution with observed mean firing rate of the unit. The minimum probability across spans of central bins has to be less than 0.05.

Behavioral task

Training took place in an operant box with three nose ports (left, center and right), and with two speakers, placed above the right and left nose ports. Each trial began with a visible light-emitting diode (LED) turning on in the center port. This cued the rat to insert its nose into the center port and keep it there until the LED was turned off (1.5 s "fixation" period). In each trial, rats were concurrently presented with two trains of auditory pulses, one train from a loudspeaker on its left, and the other from a loudspeaker on its right (Brunton et al., 2013). At the end of each trial, the subjects received a reward if they oriented to the port on the side of the auditory train with the greater total number of pulses. The timing of pulses varied both within and across individual trials and between the left and right streams. Behavioral control and stimulus generation used Bcontrol software (brodylabwiki.princeton.edu/bcontrol). Before probe implantation, subjects were trained in a semi-automated, high-throughput training facility, each in a behavioral enclosure 13" wide, 11" deep and 18.5" tall within a sound-attenuated chamber (Coulbourn). After surgery, tethered behavioral performance took place in a larger behavioral enclosure that was 13" wide, 11" deep and 40" tall within a sound-attenuated chamber and built-in Faraday cage (IAC). Untethered performance took place in the training facility, as before surgery.

Behavioral performance metrics

The performance of each rat (pooled across multiple sessions) was fit with a four-parameter logistic function:

$$P(right) = \gamma 0 + \gamma 1/(1 + exp(-\beta(x - \alpha))$$

where *x* is the click difference on each trial (number of right clicks minus number of left clicks), and *P(right)* is the fraction of trials when the animal chose right. The parameter α is x value (click difference) at the inflection point of the sigmoid, quantifying the animal's bias; β is the slope of the sigmoid at x = α, quantifying the sensitivity of the animal's choice to the stimulus; $\gamma 0$ is the minimum *P(right)*; and $\gamma 0+\gamma 1$ is the maximum *P(right)*. The lapse rate is $(1-\gamma 1)/2$. The number of trials completed excludes trials when the animal prematurely broke fixation and trials after the animal in which the animal failed to choose a side port after five seconds.

Measurement of input-referred noise

The RMS noise of the AP band (300Hz - 10kHz) of each electrode was measured in a 0.9% phosphate buffered saline (PBS) solution, following the procedure described in the Neuropixels User Manual (IMEC). To accurately compare across electrodes and probes, this procedure requires first determining a gain correction factor for each electrode, so that the nominal and actual gains match. To do this, we measured the response to a 4mVpp, 1.8kHz sine wave generated using an arbitrary waveform generator (PXIe-5413, National Instruments) in 0.9% PBS. We compared the measured amplitudes on each electrode to the amplitude measured on an independent, calibrated I/O module (PXI-6133, National Instruments) to determine the gain correction factor. Only the electrodes implanted in the brain were analyzed because a large fraction of the overlying electrodes were covered with silicone elastomer or petroleum jelly during the surgery which proved difficult to fully remove.

Choice selectivity

This metric is based on the receiver operating characteristic (ROC) and indexes how well an ideal observer can classify left- versus right-choice trials using the spike counts of an isolated unit. Spikes were counted in 0.1 s bins stepped in 0.02 s, from 1 s before movement onset to 0.5 s afterwards. Trials were included for analysis if the rat did not prematurely disengage from the center port and also reported its choice within five seconds after it was cued to do so. An ROC curve classifying left- and right-choice trials was constructed based on the spike counts of each unit in each time bin. The area under the ROC curve ranged from 0 to 1, with values greater than 0.5 indicating a larger mean spike count associated with right-choice trials. Because the present analysis concerns only the magnitude and not the directionality of the choice selectivity, a value *x* less than 0.5 was flipped to the corresponding value above 0.5, i.e. |x-0.5| + 0.5. The choice selectivity results were from the first recording session for each animal after the implantation when the animal had completed more than a hundred trials (4-11 days after surgery).

Author contributions

AGB, DG, and TZL designed the experiments. AGB, CDK, DG, and TZL collected the data. AGB, TZL, and VAE analyzed the data. AGB, CDB, and TZL wrote the manuscript.

Acknowledgements

We thank M. Schottdorf and M. Oostland for comments and discussion; J. Teran for technical assistance; J. Putzeys for advice on measurement of input-referred noise; and J. Colonell and B. Karsh for advice on the recording equipment.

References

Allen WE, Chen MZ, Pichamoorthy N, Tien RH, Pachitariu M, Luo L, Deisseroth K. 2019. Thirst regulates motivated behavior through modulation of brainwide neural population dynamics. *Science* **364**:253.

Bayly PV, Cohen TS, Leister EP, Ajo D, Leuthardt EC, Genin GM. 2005. Deformation of the human brain induced by mild acceleration. *J Neurotrauma* **22**:845–856.

Bjornsson CS, Oh SJ, Al-Kofahi YA, Lim YJ, Smith KL, Turner JN, De S, Roysam B, Shain W, Kim SJ. 2006. Effects of insertion conditions on tissue strain and vascular damage during neuroprosthetic device insertion. *J Neural Eng* **3**:196–207.

Bragin A, Hetke J, Wilson CL, Anderson DJ, Engel J Jr, Buzsáki G. 2000. Multiple site silicon-based probes for chronic recordings in freely moving rats: implantation, recording and histological verification. *J Neurosci Methods* **98**:77–82.

Brunton BW, Botvinick MM, Brody CD. 2013. Rats and humans can optimally accumulate evidence for decision-making. *Science* **340**:95–98.

Budday S, Nay R, de Rooij R, Steinmann P, Wyrobek T, Ovaert TC, Kuhl E. 2015. Mechanical properties of gray and white matter brain tissue by indentation. *J Mech Behav Biomed Mater* **46**:318–330.

Chung JE, Joo HR, Fan JL, Liu DF, Barnett AH, Chen S, Geaghan-Breiner C, Karlsson MP, Karlsson M, Lee KY, Liang H, Magland JF, Pebbles JA, Tooker AC, Greengard LF, Tolosa VM, Frank LM. 2019. High-Density, Long-Lasting, and Multi-region Electrophysiological Recordings Using Polymer Electrode Arrays. *Neuron* **101**:21–31.e5.

Chung J, Sharif F, Jung D, Kim S, Royer S. 2017. Micro-drive and headgear for chronic implant and recovery of optoelectronic probes. *Sci Rep* **7**:2773.

Davidson JD, El Hady A. 2019. Foraging as an evidence accumulation process. *PLoS Comput Biol* **15**:e1007060.

Erlich JC, Bialek M, Brody CD. 2011. A cortical substrate for memory-guided orienting in the rat. *Neuron* **72**:330–343.

Erö C, Gewaltig M-O, Keller D, Markram H. 2018. A Cell Atlas for the Mouse Brain. *Front Neuroinform* **12**:84.

Gefen A, Margulies SS. 2004. Are in vivo and in situ brain tissues mechanically similar? *J Biomech* **37**:1339–1352.

Gilletti A, Muthuswamy J. 2006. Brain micromotion around implants in the rodent somatosensory cortex. *J Neural Eng* **3**:189–195.

Harris KD, Henze D a., Csicsvari J, Hirase H, Buzsáki G. 2000. Accuracy of tetrode spike separation as determined by simultaneous intracellular and extracellular measurements. *J Neurophysiol* **84**:401–414.

Hoy JL, Bishop HI, Niell CM. 2019. Defined Cell Types in Superior Colliculus Make Distinct Contributions to Prey Capture Behavior in the Mouse. *Curr Biol* **29**:4130–4138.e5.

Ito HT, Zhang S-J, Witter MP, Moser EI, Moser M-B. 2015. A prefrontal-thalamo-hippocampal circuit for goal-directed spatial navigation. *Nature* **522**:50–55.

Jeong J-W, Shin G, Park SI, Yu KJ, Xu L, Rogers JA. 2015. Soft materials in neuroengineering for hard problems in neuroscience. *Neuron* **86**:175–186.

Juavinett AL, Bekheet G, Churchland AK. 2019. Chronically implanted Neuropixels probes enable high-yield recordings in freely moving mice. *Elife* **8**. doi:10.7554/eLife.47188

Jun JJ, Steinmetz NA, Siegle JH, Denman DJ, Bauza M, Barbarits B, Lee AK, Anastassiou CA, Andrei A, Aydın Ç, Barbic M, Blanche TJ, Bonin V, Couto J, Dutta B, Gratiy SL, Gutnisky DA, Häusser M, Karsh B, Ledochowitsch P, Lopez CM, Mitelut C, Musa S, Okun M, Pachitariu M, Putzeys J, Rich PD, Rossant C,

Sun W-L, Svoboda K, Carandini M, Harris KD, Koch C, O'Keefe J, Harris TD. 2017. Fully integrated silicon probes for high-density recording of neural activity. *Nature* **551**:232–236.
Kim Y-T, Hitchcock RW, Bridge MJ, Tresco PA. 2004. Chronic response of adult rat brain tissue to implants anchored to the skull. *Biomaterials* **25**:2229–2237.
Krupic J, Bauza M, Burton S, O'Keefe J. 2018. Local transformations of the hippocampal cognitive map. *Science* **359**:1143–1146.
Lecomte A, Descamps E, Bergaud C. 2018. A review on mechanical considerations for chronically-implanted neural probes. *J Neural Eng* **15**:031001.
Lind G, Linsmeier CE, Schouenborg J. 2013. The density difference between tissue and neural probes is a key factor for glial scarring. *Sci Rep* **3**:2942.
Luan L, Wei X, Zhao Z, Siegel JJ, Potnis O, Tuppen CA, Lin S, Kazmi S, Fowler RA, Holloway S, Dunn AK, Chitwood RA, Xie C. 2017. Ultraflexible nanoelectronic probes form reliable, glial scar-free neural integration. *Sci Adv* **3**:e1601966.
Luo TZ, Bondy AG, DePasquale B, Brody CB. 2020. The anterior dorsomedial frontal cortex is causally involved in regulating the time constant of evidence accumulation. Cosyne Abstracts, Denver, CO.
MacManus DB, Pierrat B, Murphy JG, Gilchrist MD. 2018. Region and species dependent mechanical properties of adolescent and young adult brain tissue. *Sci Rep* **8**:11234.
Mora Lopez C, Putzeys J, Raducanu BC, Ballini M, Wang S, Andrei A, Rochus V, Vandebriel R, Severi S, Van Hoof C, Musa S, Van Helleputte N, Yazicioglu RF, Mitra S. 2017. A Neural Probe With Up to 966 Electrodes and Up to 384 Configurable Channels in 0.13 μm SOI CMOS. *IEEE Trans Biomed Circuits Syst* **11**:510–522.
Muthuswamy J, Saha R, Gilletti A. 2005. Tissue micromotion induced stress around brain implants2005 3rd IEEE/EMBS Special Topic Conference on Microtechnology in Medicine and Biology. pp. 102–103.
Pachitariu M, Steinmetz N, jenniferColonell, Bondy AG, Saxena R, geffenlab, Nakamura KC, O'Shea D, Denman D, carsen-stringer, Winter O, Guzman J, Rossant C, Liddell A. 2020. MouseLand/Kilosort2: release for Zenodo DOI. doi:10.5281/zenodo.3597475
Paxinos G, Watson C. 2006. The Rat Brain in Stereotaxic Coordinates: Hard Cover Edition. Elsevier.
Polikov VS, Tresco PA, Reichert WM. 2005. Response of brain tissue to chronically implanted neural electrodes. *J Neurosci Methods* **148**:1–18.
Putzeys J, Musa S, Mora Lopez C, Raducanu BC, Carton A, De Ceulaer J, Karsh B, Siegle JH, Van Helleputte N, Harris TD, Dutta B. 2019. Neuropixels Data-Acquisition System: A Scalable Platform for Parallel Recording of 10 000+ Electrophysiological Signals. *IEEE Trans Biomed Circuits Syst* **13**:1635–1644.
Sloots JJ, Biessels GJ, Zwanenburg JJM. 2020. Cardiac and respiration-induced brain deformations in humans quantified with high-field MRI. *Neuroimage* **210**:116581.
Steinmetz NA, Zatka-Haas P, Carandini M, Harris KD. 2019. Distributed coding of choice, action and engagement across the mouse brain. *Nature* **576**:266–273.
Tervo DGR, Proskurin M, Manakov M, Kabra M, Vollmer A, Branson K, Karpova AY. 2014. Behavioral variability through stochastic choice and its gating by anterior cingulate cortex. *Cell* **159**:21–32.
The International Brain Laboratory, Aguillon-Rodriguez V, Angelaki DE, Bayer HM, Bonacchi N, Carandini M, Cazettes F, Chapuis GA, Churchland AK, Dan Y, Dewitt EE, Faulkner M, Forrest H, Haetzel LM, Hausser M, Hofer SB, Hu F, Khanal A, Krasniak CS, Laranjeira I, Mainen ZF, Meijer GT, Miska NJ, Mrsic-Flogel TD, Murakami M, Noel J-P, Pan-Vazquez A, Sanders JI, Socha KZ, Terry R, Urai AE, Vergara HM, Wells MJ, Wilson CJ, Witten IB, Wool LE, Zador A. 2020. A standardized and reproducible method to measure decision-making in mice. *bioRxiv*. doi:10.1101/2020.01.17.909838
Wood F, Black MJ, Vargas-Irwin C, Fellows M, Donoghue JP. 2004. On the variability of manual spike sorting. *IEEE Trans Biomed Eng* **51**:912–918.
Zhou R, Li Y, Cavanaugh JM, Zhang L. 2020. Investigate The Variations Of The Head And Brain Response In A Rodent Head Impact Acceleration Model By Finite Element Modeling. *Frontiers in Bioengineering and Biotechnology* **8**:172.